Desalination and Water Treatment
www.deswater.com

doi: 10.5004/dwt.2017.21196

84 (2017) 205–214
July

Low-cost and eco-friendly activated carbon from modified palm kernel shell for hydrogen sulfide removal from wastewater: adsorption and kinetic studies

Omar Abed Habeeb[a,b], K. Ramesh[a,*], Gomaa A.M. Ali[c,d,e], Rosli bin Mohd Yunus[a]

[a]*Faculty of Chemical & Natural Resources Engineering, Universiti Malaysia Pahang, Gambang 26300, Kuantan, Malaysia, emails: ramesh@ump.edu.my (K. Ramesh), omer_habeeb2003@yahoo.com (O.A. Habeeb), rmy@ump.edu.my (R.M. Yunus)*
[b]*North Refinery Company, Ministry of Oil of Iraq, Baiji, Salahaldeen 34007, Iraq*
[c]*Faculty of Industrial Sciences & Technology, Universiti Malaysia Pahang, Gambang 26300 Kuantan, Malaysia, emails: gomaasanad@azhar.edu.eg, gomaasanad@gmail.com (G.A.M. Ali)*
[d]*Chemistry Department, Faculty of Science, Al-Azhar University, Assiut 71524, Egypt*
[e]*Al-Azhar Center of Nanoscience and Applications (ACNA), Al-Azhar University, Assiut 71524, Egypt*

Received 2 January 2017; Accepted 10 July 2017

ABSTRACT

Palm kernel shell is an abundant agricultural by-product in Malaysia, which is mainly used for producing activated carbon (AC) via the process called physicochemical activation. The applicability of AC derived from palm kernel shell (ACPKS) was investigated for the removal of dissolved H_2S from wastewater. ACPKS was characterized by energy-dispersive X-ray, Fourier transform infrared spectroscopy, Brunauer–Emmett–Teller surface area and scanning electron microscope. The batch mode was utilized for studying adsorption capacity. The effects of various parameters were evaluated and these parameters were then optimized. Parameters such as initial concentration (500 mg/L), dose (100 mg/L), pH (7), agitation speed (150 rpm) and contact time (14 h) for removing dissociated H_2S were optimized. Equilibrium data for H_2S adsorption on ACPKS were fitted using the Langmuir, Freundlich, Temkin, and Dubinin–Radushkevich isotherm models. The experimental data were comparable to the predictions of Langmuir equation, where the maximum monolayer adsorption capacity of 524.2 mg/g was found. The pseudo-first-order, pseudo-second-order, and intraparticle diffusion models were employed for simulating the experimental data for the adsorption kinetics. Among these models, the pseudo-first-order model was the best fitting model based on the correlation coefficients (R^2) and normalized standard deviation (sum of squared error). The current study shows that ACPKS is the promising adsorbent for removing H_2S from wastewater and other aqueous solutions.

Keywords: Palm kernel shell; Hydrogen sulfide; Activated carbon; Adsorption isotherms; Water treatment; Kinetics

1. Introduction

The increase in global gasoline consumption has caused petroleum refineries to produce enormous amounts of refined products. Meanwhile, the crude oil refining process is often associated with production of wastewater. Typically, high-strength wastewater is released from petroleum refineries, which contains high concentrations of inorganic and organic contaminants such as phenol, amines, cyanides, and hydrogen sulfide (H_2S). Among these contaminants, H_2S is highly hazardous, which would cause pipeline corrosion and pose a high health risk when it is released to the environment even at low concentration [1–4]. Depending on its concentration, H_2S may cause many health problems such as paralysis of respiration and respiratory arrest, central nervous system stimulation, pulmonary edema, eye damage and threshold for eye irritation [5]. Human nose can detect the rotten egg

* Corresponding author.

odor (consists of low H_2S concentration at 0.0047 ppm) [5,6]. Therefore, researchers have developed different techniques for removing H_2S from wastewater such as precipitation [7], reduction [8], oxidation [3,9] and adsorption [4,10]. Amongst these techniques, adsorption is the most common method.

Activated carbon (AC) is a solid, porous and black carbonaceous material. It is the main adsorbent used in industries for wastewater treatment. It can be obtained from enormous carbon-based solid precursors, either synthetic or natural. Carbon is typically a functional material with high market value, which is obtained from petroleum coke, pitch and coal. These carbonaceous materials are non-renewable. Hence, it is imperative to identify suitable alternatives such as agricultural wastes [11,12]. In addition, the development of AC from waste bio-resources results in two concurrent effects: environmental remediation and wealth creation [12,13]. Several studies have been reported on producing AC from agricultural wastes such as nut shell [14], sugarcanes [15], almond shell [16], fruit stones [17], coconut shell [18], macadamia nut shells [19], fibers of oil palm empty fruit bunches [20], rice straw [21], sunflower straw [22], cotton stalk [23] and date stones [24]. However, only a few studies have been conducted on using palm kernel shell (PKS) residue [25,26]. Prior to the use of AC derived from PKS, it is imperative to activate it either by chemical or physical methods. The chemical route consists of the impregnation of carbonaceous precursors via heating with chemical reagent (mostly KOH and $ZnCl_2$) [27,28]. On the other hand, physical method involves carbonization of raw material, followed by controlled gasification in a stream of oxidizing agents such as steam, CO_2, or air [29]. Chemical and physical methods employ KOH and CO_2 as activators, respectively, to enhance the adsorption capacity of AC derived from PKS.

In this study, AC was produced from PKS waste residue by physicochemical activation using KOH and CO_2. This study aims to evaluate the potential of PKS-based AC to adsorb H_2S in a simulated wastewater. Moreover, the kinetics and isotherm equilibrium models of adsorption process were investigated in order to understand the H_2S adsorption mechanism of palm kernel-based AC.

2. Materials and methods

2.1. Activated carbon preparation

Palm kernel shell (PKS) waste residue was obtained from United Palm Oil Mill, Nibong Tebal, Malaysia. First, the PKS was washed with deionized water in order to remove soils and other impurities. Subsequently, the washed PKS was air-dried to remove water. This was followed by mechanical grinding and sieving to produce particles of size ranging from 0.5 to 1 mm. These particles were further dried at 110°C for 24 h. The PKS was subjected to a pyrolysis process performed at 700°C for 2 h in an inert atmosphere (N_2 flow of 150 mL/min) for the production of char using a tubular horizontal reactor (nominal diameter of 2 inches). Batches of 20 g sample were utilized in each experiment. The yield of the carbon produced can be calculated as: yield (%) = 100 × (W_c/W_o), where W_c and W_o are the dry weights of the final sample and the precursor, respectively. The AC yield was found to be 43.17%.

The absence of sulfur and low ash content in char are positive factors, making PKS a good starting material for the production of AC. The resulting carbon was mixed with KOH at an optimum char/KOH ratio of 1:4 suggested by previous researchers [30,31]. The mixture was left for 24 h and filtered. The filtered carbon was placed in the tubular horizontal reactor and gradually heated with inert gas (N_2 flow of 150 mL/min) until the maximum temperature of 750°C was attained. Then, the N_2 gas was switched to CO_2 gas for 2 h. The AC produced was cooled and washed using boiled deionized water with HCl for 1 h in order to remove the residual KOH. Finally, the sample was washed several times with distilled water in order to reach the normal pH condition. The final product was dried at 110°C for 24 h and coded as ACPKS.

2.2. Activated carbon characterizations

Thermal analyses (e.g., thermogravimetric analysis (TGA) and differential thermal analysis (DTA)) were performed with the TA Instruments (Q500) thermal analyzer at 800°C (heating rate of 10°C/min in N_2 environments). Fourier transform infrared spectroscopy (FTIR) was mainly employed as a qualitative technique for evaluating the chemical structure of carbon materials. FTIR spectra were recorded between 4,000 and 400 cm^{-1} in order to examine the functional groups on the surface of the modified sample (ACPKS). FTIR analysis was performed using JASCO-480 Plus. The porous structure of the AC particles was investigated by N_2 adsorption–desorption isotherms at −196°C using the ASAP 2020 apparatus (Micromeritics Co., USA). The specific surface area (S_{BET}, m^2/g) and the total pore volume (V_t, cm^3/g at standard temperature and pressure) of ACPKS were obtained using Brunauer–Emmett–Teller (BET) and Barrett–Joyner–Halenda (BJH) methods. The actual density (ρ) of the sample was measured by the helium displacement method using the AccuPyc II 1340 pycnometer (Micromeritics Co., USA). Scanning electron microscopy (SEM) was employed for investigating the textural morphologies of ACPKS. SEM was conducted using the HITACHI TM3030, Japan system running at an accelerating potential of 20 kV. Elemental analysis or the chemical characterization of samples was analyzed by energy-dispersive X-ray (EDX) spectroscopy in order to examine the interaction between an X-ray excitation source and a sample.

2.3. Preparation of H_2S solutions

In this study, synthetic wastewater was prepared in accordance with the procedure reported by Asaoka et al. [32]. First, a known amount of $Na_2S{\cdot}9H_2O$ was dissolved in a 500 mL solution of 0.01 M KCl purged with N_2. Second, the solution pH was adjusted to 7 using 0.2 M HCl [32]. H_2S in solution can exist in three forms: H_2S, HS^- and S^{2-} [33].

2.4. Batch equilibrium studies

The experiments for H_2S adsorption were conducted in the batch mode. ACPKS was intensively examined for investigating its ability to adsorb dissolved H_2S from synthetic wastewater. A sample of 100 mg of an adsorbent was used in each run after degassing at 105°C for 24 h in an oven.

The adsorption experiments were performed in a set of 250-mL Erlenmeyer flasks containing 100 mg of ACPKS and 100 mL of H_2S solutions at various initial concentrations (100, 200, 300, 400 and 500 mg/L), mimicking the studies performed earlier [34,35]. The flasks were agitated in a thermostatic orbital shaker at 150 rpm and 30°C until the equilibrium was reached. The concentrations of H_2S in the supernatant solutions were measured by spectrophotometer HACH DR2800 using sulfide reagent 1&2 (method: methylene blue).

The ACPKS adsorption capacity (q_e mg/g) was calculated using equation: $q_e = (C_o - C_e)V/m$ [36,37]. Subsequently, the initial and the final concentrations were measured after the suspensions were filtered. Here, V is the solution volume (L), m is the adsorbent amount (g) and C_o and C_e are the initial and the final H_2S concentrations, respectively. All adsorption experiments were repeated two times, and we found that the maximum deviation was ~5%. All measurements and experiments were conducted in a fume hood as H_2S is a very dangerous gas.

2.5. Adsorption isotherm models

Typically, an adsorption isotherm is an oriental graph describing the phenomenon governing the retention of a substance from aquatic environment on a solid phase at constant temperature [38,39]. Generally, the adsorption isotherm governs the relation between the amount of adsorbate adsorbed per unit mass of adsorbent (q_e) and the concentration of adsorbate at equilibrium conditions (C_e). The well-known isotherm models such Langmuir [40–42], Freundlich [40,43,44], Temkin [45,46] and Dubinin–Radushkevich [47,48] models were applied and the relevant parameters were then calculated.

2.6. Batch kinetic studies

In addition to isotherm studies, adsorption kinetics was carried out for simulating the uptake of H_2S by adsorbents. For investigating the adsorption kinetics of H_2S on adsorbent, pseudo-first-order [36,49], pseudo-second-order [46,50] and intraparticle diffusion [36] models were employed for simulating the experimental data.

2.7. Validity of kinetic model

Besides the R^2 value, all kinetic models were verified by normalized standard deviation or sum of squared error (SSE, %). The validity of each model was determined by SSE using the equation reported elsewhere [37,51]. Better fitting model is characterized by higher R^2 and lower SSE values.

3. Results and discussion

3.1. Textural characteristics of ACPKS

Thermal analyses of ACPKS were performed in order to choose the suitable carbonization temperature. As shown in Fig. 1, TGA shows the weight loss of 17.65% and the DTA peak at less than 100°C due to the removal of adsorbed surface water. At 600°C, it shows other weight loss of 12.14% together with the DTA peak of low intensity due to the removal of CO_2 and other materials [52,53]. Between 600°C and 800°C, ACPKS shows a thermal stable carbon structure. Therefore, 700°C was chosen as the carbonization temperature.

FTIR has been widely employed for characterizing the surface groups of oxides and carbonaceous materials. Fig. 2 shows the FTIR spectrum of ACKPS before and after the adsorption process. Bands located at 3,450, 2,160 and 2,030 cm^{-1} correspond to O–H stretching, C=C stretching and C–O stretching vibrations, respectively. These bands are observed in both materials before and after the process, indicating that the carbon structure was not destroyed during the sulfur adsorption. C–O stretching vibrations are probably attributed to the surface functional groups of ACPKS that are dominated by carbon material. On the other hand, the ACKPS after adsorption shows additional band at 911 cm^{-1}, which is related to the C–S bond stretching [54]. This indicates the accumulation of S on the carbon surface. The acidity and the basicity of surfaces can be used to describe the surface chemistry of carbon adsorbent. Surface basicity is related to the presence of oxygen-free Lewis sites as well as those carbonyls, pyrone and chromene-type structures at the edge of the carbon layers. On the other hand, the acidic behavior is associated with the oxygen-containing groups (mainly carboxylic acid, anhydrides, lactones and phenols). Chemical activation using KOH as an activation agent could possibly increase the basic groups, which is attributed to the increase of strongly basic hydroxyl group (OH^-) on the surface [55].

Fig. 3 displays the N_2 adsorption/desorption isotherm of ACPKS and the inset shows the pore size distribution. As seen, ACPKS shows high specific surface area based on

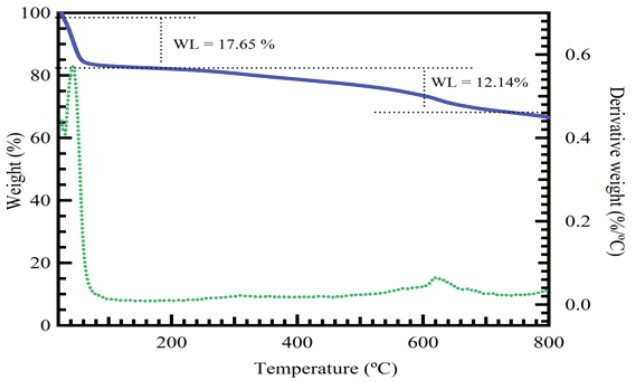

Fig. 1. TGA (solid line) and DTA (dotted line) of ACPKS.

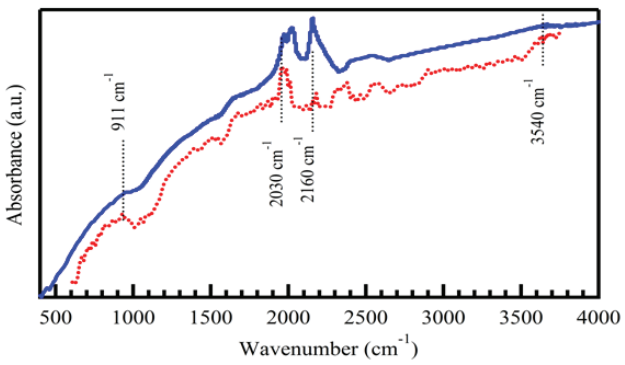

Fig. 2. FTIR spectrum of ACKPS before (solid line) and after (dotted line) the adsorption process.

BET theory (S_{BET} value of 776.4 m^2/g). The average pore width (P_w) is related to S_{BET} and pore volume (V_p) as: $P_w = 4V_p/S_{BET}$ [56]. The total pore volume of ACPKS was 0.34 cm^3/g and the average pore diameter was 2.3 nm. This large pore diameter is suitable for H_2S removal. The actual density of ACPKS was estimated as 2.217 g/cm^3. Consequently, the void fraction or porosity of ACPKS (ε,%) was 43% according to the expression $\varepsilon = V_p/V_p + 1/\rho$ [57,58]. Therefore, ACPKS is efficient in adsorption process due to its high void fraction and porosity. Other parameters derived from N_2 adsorption/desorption data are listed in Table 1. The large surface area and porous structure of ACPKS are attributed to chemical and physical activations using KOH and CO_2, respectively. The reactions such as KOH–carbon and CO_2–carbon could possibly create more pores in the ACPKS structure. Pore generation works based on dehydration of KOH to K_2O, which reacts with CO_2 produced by the water shift reaction, thus forming K_2CO_3 as well as promoting the diffusion of KOH and CO_2 molecules into the pores (hence, increased porosity [31]). In addition, adsorbents with large portions of mesopores could favor the formation of water film to facilitate the chemisorption of H_2S and high sulfur content. Moreover, metallic potassium appeared to be responsible for the drastic increase of carbon material, resulting in pore formation and increased pore volume [59].

Fig. 4(a) shows the microscopic structure of fresh ACPKS in SEM image. Large pores are evident on the AC surface, indicating that the carbonization stage mainly creates macro- and mesoporous carbons. After adsorption, the pores are seemingly filled by sulfur as less porosity is observed (see Fig. 4(b)). In addition, EDX analyses were performed on fresh and used materials as shown in Figs. 4(c) and (d), respectively. The EDX chart for the fresh ACPKS adsorbent shows peaks that correspond to C, O and K. For the used ACPKS, peaks that correspond to C, O, K, S, Na and Al are observed. In addition, the intensity of peak corresponding to S is quite high, indicating that the efficiency of the current removal process is indeed promising.

Table 2 summarizes the content of ACPKS before and after adsorption. As observed, the components were changed after adsorption. The fresh adsorbent contains components such as C, O and K (the percentages are 73.41%, 18.71%, and 7.88%, respectively). However, components such as S, Na and Al are not observed. The change in components of the adsorbent is probably attributed to oxidation and adsorption. The most interesting finding is that the percentage of K decreases to around 0.25% after adsorption, indicating that acid–base reaction occurs. The presence of Al (although low in percentage) might be due to the aluminum paper used during the sampling process. Meanwhile, the Na component might be produced from the dissolution of sodium sulfide: $Na_2S + H_2O \rightarrow H_2S$ (aq) + 2NaOH. On the other hand, the percentage of S content is 7.41%, showing the adsorption of sulfur compounds on AC.

Table 1
Specific surface area and other related parameters of ACPKS

Properties	Value
BET surface area (m^2/g)	776.4
Micropore surface area (m^2/g)	168.4
Total pore volume (cm^3/g)	0.34
Void fraction or porosity (%)	43
Mesopore volume (cm^3/g)	0.16
Average pore size (nm)	3.99

3.2. Effect of contact time and initial H_2S concentration on adsorption equilibrium

Moisture can enhance the removal efficiency of H_2S(g) due to the dissociation of H_2S(g) to H_2S(aq) at the boundary layer of the adsorbent surface. This makes them easily attracted on the active sites of adsorbent. Thus, it is easier to remove H_2S in its ionic forms (H_2S(aq)) such as bisulfide (HS^-) and sulfide (S^{2-}) instead of its gaseous form [60]. In addition, moisture facilitates the complete oxidation of H_2S into SO_4^{2-}, causing no secondary pollution [61]. Therefore, this study focuses on removing H_2S(aq) using AC produced from waste materials.

Typically, the adsorption capacity of H_2S and the adsorbent efficiency increase with increasing contact time. Fig. 5 shows the adsorption capacity vs. adsorption time at various initial H_2S concentrations at 30°C. As observed, the H_2S solutions of initial concentrations 100–500 mg/L would take 8–10 h to reach equilibrium. However, the experiment was performed up to 14 h to ensure complete equilibrium. The results indicate that contact time plays an important role in adsorption. As observed from Fig. 5, initially, the amount of H_2S adsorbed onto the carbon surface increases steadily. After certain time, the process decelerates and the adsorbed amount plateaus (equilibrium). At the initial concentration range of 100–200 mg/L, shorter time is required to reach the equilibrium, due to the fact that there are many empty sites that can be used to trap the H_2S molecules, as well as several active functional groups (OH^-) on the adsorbent surface at the beginning of adsorption. In fact, Fig. 5 indicates that the acid/base reaction occurs on the adsorbent surface, which is attributed to the basic functional groups on the adsorbent surface. This reaction can enhance the adsorption of acidic pollutant (e.g., H_2S). As reported in Fig. 5, the sulfur percentage increases rapidly as well. Thus, the amount of H_2S

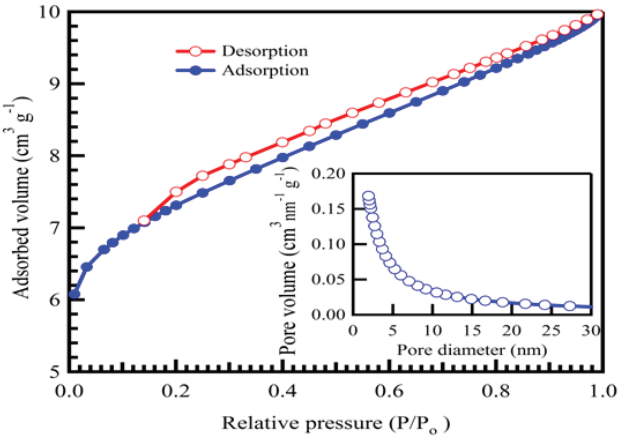

Fig. 3. N_2 adsorption-desorption isotherm of ACPKS: the inset shows the pore size distribution.

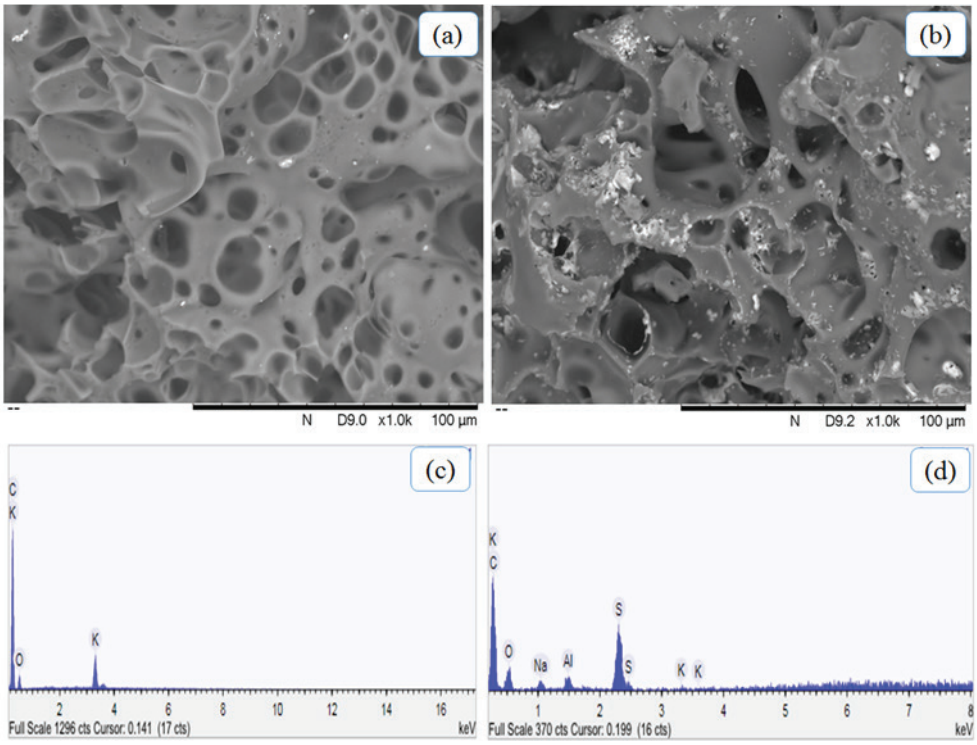

Fig. 4. SEM images (a) and (b) and EDX (c) and (d) for ACPKS before and after adsorption process, respectively.

Table 2
Elemental components of fresh and used adsorbent

Element	Fresh adsorbent (wt%)	Spent adsorbent (wt%)
C	73.41	72.55
O	18.71	17.61
K	7.88	0.25
Al	Not detected	1.12
Na	Not detected	1.06
S	Not detected	7.41

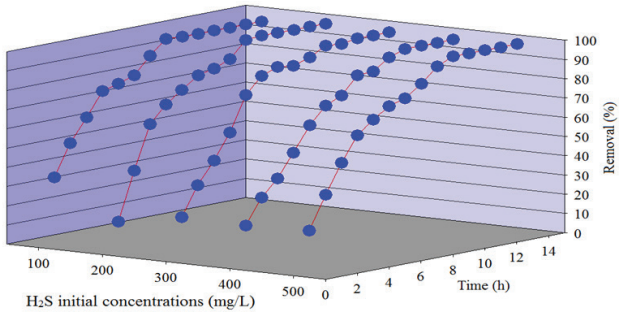

Fig. 5. Variation of removal percentage with adsorption time at various H_2S initial concentrations at 100 mg dosage, 30°C and pH of 7 and 150 rpm.

adsorbed on AC indicates the adsorption capacity of adsorbent. In this study, the adsorption equilibrium q_e increases from 94 to 490 mg/g as the initial concentration increases from 100 to 500 mg/L (see Fig. 4). The mechanisms of adsorption could be explained by three consecutive mass transport steps. First, the adsorbate migrates through the solution, that is, film diffusion, followed by the movement of solute from the particle surface into the interior site by pore diffusion. Finally, the adsorbate is adsorbed into the active sites at the interior of adsorbent particle.

3.3. Adsorption isotherms

Adsorption isotherms are essential for describing the manner in which solutes interact with adsorbents. Moreover, it shows the distribution of adsorbed molecules between solid and liquid phases and the time taken to reach an equilibrium state. Fitting of different isotherm models is an important step for finding a suitable model that can be used for design purposes [62]. Here, Langmuir, Freundlich, Temkin, and Dubinin–Radushkevich isotherm models were applied. As shown in Fig. 6(a), the Langmuir adsorption isotherm model is suitable for representing the adsorption process of H_2S on ACPKS. For the Langmuir isotherm, the straight line with a slope of $1/Q_o$ is obtained from the plot of C_e/q_e against C_e (see Fig. 6). The Langmuir constants b and Q_o are calculated and shown in Table 3. An R^2 value of 0.9912 indicates that the adsorption data of H_2S on ACPKS are well fitted to the Langmuir isotherm model. The maximum adsorption capacity is found to be 524.2 mg/g that is relatively high compared with those reported by other studies as shown in Table 4. The high adsorption capacity is related to high void fraction, porous nature, high surface area and activation of the surface of ACPKS. The R_L value is another evidence to support this inference, which is calculated as

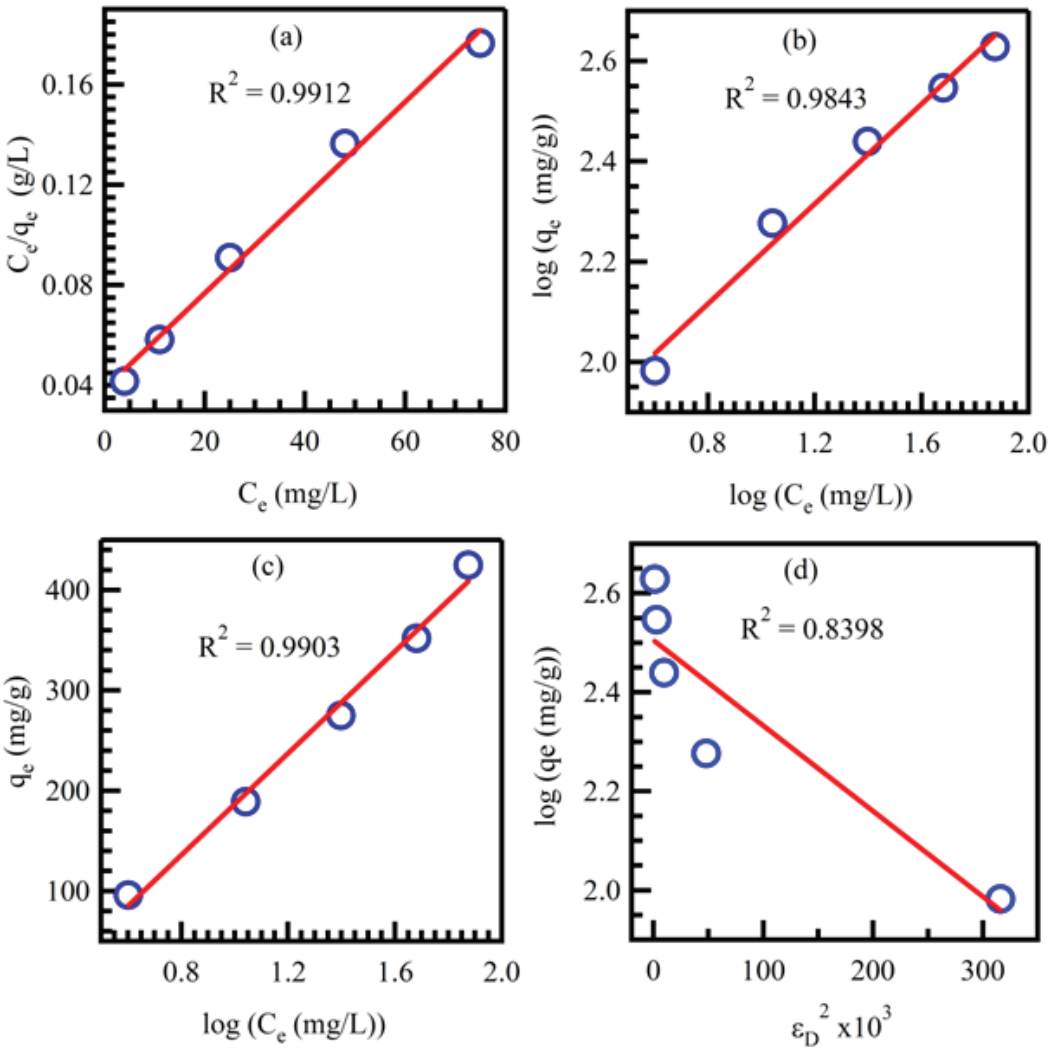

Fig. 6. Langmuir (a), Freundlich (b), Temkin (c) and Dubinin–Radushkevich (d) adsorption isotherms of H_2S on ACPKS at 30°C.

Table 3
Parameters of different isotherm models and correlation coefficients for the adsorption of H_2S on ACKPS

Isotherm model	Parameter	Value	R^2
Langmuir	Q_{max} (mg/g)	524.2	0.9912
	K_l (L/mg)	0.0495	
Freundlich	K_F (mg/g(L/mg)$^{1/n}$	52.13	0.9843
	$1/n$	0.4982	
Temkin	K_T (L/g)	0.766	0.9903
	B_T (J/mol)	9.92	
Dubinin–Radushkevich	q_s (mg/g)	12.2	0.8398
	k_D (mol/J)^2	1.7×10^{-6}	
	E (J/mol)	538.2	

0.03882 at a particular solution concentration. This further confirms that Langmuir isotherm is favorable for describing the adsorption of H_2S on ACPKS under the conditions employed in this study.

For the Freundlich isotherm, a straight line with a slope of $1/n$ (value of 0.4982) is obtained from the plot of logq_e vs. logC_e (see Fig. 6(b)). This result demonstrates that the adsorption of H_2S on ACPKS is favorable. However, the R^2 value is 0.9843, indicating that the fitting of adsorption data is not as good as that of the Langmuir model. Accordingly, the Freundlich constants K_F and n are calculated and listed in Table 3.

For the Temkin isotherm model, the linear relation between q_e and logC_e is shown in Fig. 6(c), and the fitting parameters are shown in Table 3. However, the R^2 value of Temkin isotherm model is 0.9903, indicating that the adsorption data of H_2S on ACPKS is more or less fitted. A smaller R^2 value of 0.8389 is obtained for the Dubinin–Radushkevich isotherm. A straight line is obtained from the plot of logq_e vs. ε_D^2 (Fig. 6(d)). The constants q_s and E are determined and reported in Table 3.

3.4. Adsorption kinetics

For the pseudo-first-order kinetic model, straight lines are obtained by plotting log($q_e - q_t$) vs. t as shown

Table 4
Adsorption capacities of H_2S on various adsorbents and palm kernel shell AC for various pollutants

Adsorbents	Pollutants	Adsorption capacity (mg/g)	S_{BET} (m^2/g)	References
AC from sawdust pellets	H_2S	6.2	426	[63]
Carbonated steel slag		7.5	14.4	[64]
Impregnated AC		9.4	732	[65]
Sewage sludge/fish waste mixture		22	25	[66]
Graphite-derived materials		30.5	192	[67]
AC/bentonite binders		47	1410	[68]
AC from oil–palm shell		76	1062	[6]
N_2-modified carbide AC		90.5	1297	[69]
Adsorption/oxidation on unmodified AC		112	1063	[70]
Bituminous-coal-based AC		256	661	[71]
CaO/ACPKS		543.47	476.7	[37]
Palm kernel shell AC	Methylene blue	40–110	1268	[72]
	Phenol	78–82		
	Cr(VI)	0.35–0.37		
	Basic blue 9	333.33	1088	[73]
	Lead	1.337	513.3	[74]
	Copper	1.581		
	Nickel	0.130		
ACPKS	H_2S	524.2	776.4	This study

in Fig. 7(a). On the other hand, when the pseudo-second-order kinetic model is applied, the t/q_t vs. t plot shows a linear relationship as shown in Fig. 7(b). Then, k_2 can be determined from the intercept of the plot. This procedure is more likely to predict the behaviour over the whole range of adsorption. Moreover, the intraparticle diffusion model rate constant (K_{ip}) is obtained from the slope of the straight line of plot qt vs. $t^{1/2}$ (see Fig. 7(c)). The SSE value serves as an indicator for finding which kinetic model fits the adsorption process well. The SSE ranges from 3.28% to 3.82% for the pseudo-first-order kinetic model, which is lower than that of the pseudo-second-order kinetic model (8.08%–99.55%) for initial concentrations ranging from 100 to 500 mg/L. Moreover, the pseudo-first-order kinetic model fits the experimental data better due to higher R^2 value. Table 5 summarizes the calculated parameters. The adsorption of H_2S on ACPKS is best described by the first-order kinetic model.

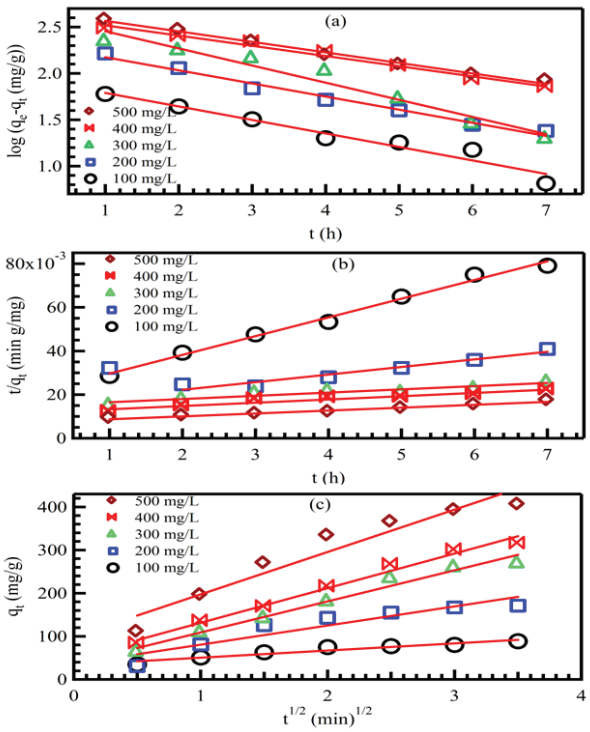

Fig. 7. Pseudo-first-order (a), pseudo-second-order (b) and intra-particle diffusion (c) kinetic models for the adsorption of H_2S on ACPKS at 30°C.

4. Conclusions

In this study, PKS is effective for preparing the activated carbon (AC). The prepared AC shows high porous structure with high specific surface area of 776.4 m^2/g, indicating that AC is an effective material for adsorption. The prepared AC has been tested over a wide range of initial concentrations. H_2S has been found to be strongly adsorbed on the AC surface due to its porous structure and high surface area. The adsorption behavior can be well described by a monolayer Langmuir isotherm. The maximum adsorption capacity (Q_{max}) has been found to be 524.2 mg/g. The kinetic data have followed the pseudo-first-order kinetic model. This study shows that the AC derived from PKS is an excellent material for wastewater treatment.

Table 5
Pseudo-first-order, pseudo-second-order, intraparticle diffusion kinetic models parameters as well as correlation coefficients for the adsorption of H_2S on ACPKS

Kinetic model	Parameter	Initial H_2S concentration (mg/L)				
		100	200	300	400	500
Pseudo-first-order kinetic model	K_1 (1/h)	0.335	0.325	0.425	0.253	0.260
	R^2	0.9536	0.9578	0.9832	0.9819	0.9904
Pseudo-second-order kinetic model	K_2 (g/mg h)	35×10^{-4}	1.8×10^{-4}	1.46×10^{-4}	1.89×10^{-4}	2.4×10^{-4}
	R^2	0.9913	0.511	0.8934	0.9187	0.9768
Intraparticle diffusion kinetic model	K_{ip} (mg/g $h^{1/2}$)	16.600	44.350	72.140	80.285	98.214
	R^2	0.9232	0.8675	0.9770	0.9855	0.9281

Acknowledgment

This work was funded by Faculty of Chemical & Natural Resources Engineering, Universiti Malaysia Pahang through an internal research grant scheme.

References

[1] A.M. Montebello, M. Fernández, F. Almenglo, M. Ramírez, D. Cantero, M. Baeza, D. Gabriel, Simultaneous methylmercaptan and hydrogen sulfide removal in the desulfurization of biogas in aerobic and anoxic biotrickling filters, Chem. Eng. J., 200 (2012) 237–246.
[2] C. Rattanapan, P. Boonsawang, D. Kantachote, Removal of H_2S in down-flow GAC biofiltration using sulfide oxidizing bacteria from concentrated latex wastewater, Bioresour. Technol., 100 (2009) 125–130.
[3] Q. Chen, J. Wang, X. Liu, Z. Li, W. Qiao, D. Long, L. Ling, Structure-dependent catalytic oxidation of H_2S over Na_2CO_3 impregnated carbon aerogels, Microporous Mesoporous Mater., 142 (2011) 641–648.
[4] W.P. Cheng, J.Z. Zhao, J.G. Yang, MgAlFeCu mixed oxides for SO_2 removal capacity: influence of the copper and aluminum incorporation method, Catal. Commun., 23 (2012) 1–4.
[5] H. Kimura, Hydrogen Sulfide and Its Therapeutic Applications, Springer, 2013.
[6] J. Guo, Y. Luo, A.C. Lua, R.-a. Chi, Y.-l. Chen, X.-t. Bao, S.-x. Xiang, Adsorption of hydrogen sulphide (H_2S) by activated carbons derived from oil-palm shell, Carbon, 45 (2007) 330–336.
[7] S. Ma, A. Noble, D. Butcher, R.E. Trouwborst, G.W. Luther, Removal of H_2S via an iron catalytic cycle and iron sulfide precipitation in the water column of dead end tributaries, Estuarine Coastal Shelf Sci., 70 (2006) 461–472.
[8] R.H.O. Montes, E.M. Richter, R.A.A. Munoz, Low-potential reduction of sulfite at a ruthenium-oxide hexacyanoferrate modified electrode, Electrochem. Commun., 21 (2012) 26–29.
[9] N. Diez, P. Alvarez, M. Granda, C. Blanco, G. Gryglewicz, I. Wróbel-Iwaniec, A. Sliwak, J. Machnikowski, R. Menendez, Tailoring micro-mesoporosity in activated carbon fibers to enhance SO_2 catalytic oxidation, J. Colloid Interface Sci., 428 (2014) 36–40.
[10] L. Zhao, X. Li, Z. Qu, Q. Zhao, S. Liu, X. Hu, The NiAl mixed oxides: the relation between basicity and SO_2 removal capacity, Sep. Purif. Technol., 80 (2011) 345–350.
[11] A. Kumar, G. Hegde, S.A.B.A. Manaf, Z. Ngaini, K.V. Sharma, Catalyst free silica templated porous carbon nanoparticles from bio-waste materials, Chem. Commun., 50 (2014) 12702–12705.
[12] G.A.M. Ali, S.A.B.A. Manaf, A. Kumar, K.F. Chong, G. Hegde, High performance supercapacitor using catalysis free porous carbon nanoparticles, J. Phys. D: Appl. Phys., 47 (2014) 495307–495313.
[13] G.A.M. Ali, S.A.A. Manaf, D. A, K.F. Chong, G. Hegde, Superior supercapacitive performance in porous nanocarbons, J. Energy Chem., 25 (2016) 734–739.
[14] Z. Hu, E.F. Vansant, Carbon molecular sieves produced from walnut shell, Carbon, 33 (1995) 561–567.
[15] T.E. Rufford, D. Hulicova-Jurcakova, K. Khosla, Z. Zhu, G.Q. Lu, Microstructure and electrochemical double-layer capacitance of carbon electrodes prepared by zinc chloride activation of sugar cane bagasse, J. Power Sources, 195 (2010) 912–918.
[16] A. Marcilla, S. Garcıa-Garcıa, M. Asensio, J.A. Conesa, Influence of thermal treatment regime on the density and reactivity of activated carbons from almond shells, Carbon, 38 (2000) 429–440.
[17] M. Kazemipour, M. Ansari, S. Tajrobehkar, M. Majdzadeh, H.R. Kermani, Removal of lead, cadmium, zinc, and copper from industrial wastewater by carbon developed from walnut, hazelnut, almond, pistachio shell, and apricot stone, J. Hazard. Mater., 150 (2008) 322–327.
[18] K. Yang, J. Peng, C. Srinivasakannan, L. Zhang, H. Xia, X. Duan, Preparation of high surface area activated carbon from coconut shells using microwave heating, Bioresour. Technol., 101 (2010) 6163–6169.
[19] A.C. Martins, O. Pezoti, A.L. Cazetta, K.C. Bedin, D.A.S. Yamazaki, G.F.G. Bandoch, T. Asefa, J.V. Visentainer, V.C. Almeida, Removal of tetracycline by NaOH-activated carbon produced from macadamia nut shells: kinetic and equilibrium studies, Chem. Eng. J., 260 (2015) 291–299.
[20] R. Farma, M. Deraman, A. Awitdrus, I.A. Talib, E. Taer, N.H. Basri, J.G. Manjunatha, M.M. Ishak, B.N.M. Dollah, S.A. Hashmi, Preparation of highly porous binderless activated carbon electrodes from fibres of oil palm empty fruit bunches for application in supercapacitors, Bioresour. Technol., 132 (2013) 254–261.
[21] P. Gao, Z.-h. Liu, G. Xue, B. Han, M.-h. Zhou, Preparation and characterization of activated carbon produced from rice straw by $(NH_4)_2HPO_4$ activation, Bioresour. Technol., 102 (2011) 3645–3648.
[22] K.Y. Foo, B.H. Hameed, Preparation and characterization of activated carbon from sunflower seed oil residue via microwave assisted K_2CO_3 activation, Bioresour. Technol., 102 (2011) 9794–9799.
[23] M. Chen, X. Kang, T. Wumaier, J. Dou, B. Gao, Y. Han, G. Xu, Z. Liu, L. Zhang, Preparation of activated carbon from cotton stalk and its application in supercapacitor, J. Solid State Electrochem., 17 (2013) 1005–1012.
[24] M.L. Sekirifa, M. Hadj-Mahammed, S. Pallier, L. Baameur, D. Richard, A.H. Al-Dujaili, Preparation and characterization of an activated carbon from a date stones variety by physical activation with carbon dioxide, J. Anal. Appl. Pyrolysis, 99 (2013) 155–160.
[25] A.C. Lua, J. Guo, Activated carbon prepared from oil palm stone by one-step CO_2 activation for gaseous pollutant removal, Carbon, 38 (2000) 1089–1097.
[26] I.I. Misnon, N.K.M. Zain, R.A. Aziz, B. Vidyadharan, R. Jose, Electrochemical properties of carbon from oil palm kernel shell for high performance supercapacitors, Electrochim. Acta, 174 (2015) 78–86.

[27] D. Lozano-Castelló, J.M. Calo, D. Cazorla-Amorós, A. Linares-Solano, Carbon activation with KOH as explored by temperature programmed techniques, and the effects of hydrogen, Carbon, 45 (2007) 2529–2536.
[28] F. Caturla, M. Molina-Sabio, F. Rodríguez-Reinoso, Preparation of activated carbon by chemical activation with $ZnCl_2$, Carbon, 29 (1991) 999–1007.
[29] A. Ahmadpour, D.D. Do, The preparation of active carbons from coal by chemical and physical activation, Carbon, 34 (1996) 471–479.
[30] M.J. Ahmed, S.K. Theydan, Physical and chemical characteristics of activated carbon prepared by pyrolysis of chemically treated date stones and its ability to adsorb organics, Powder Technol., 229 (2012) 237–245.
[31] G.G. Stavropoulos, A.A. Zabaniotou, Production and characterization of activated carbons from olive-seed waste residue, Microporous Mesoporous Mater., 82 (2005) 79–85.
[32] S. Asaoka, T. Yamamoto, S. Kondo, S. Hayakawa, Removal of hydrogen sulfide using crushed oyster shell from pore water to remediate organically enriched coastal marine sediments, Bioresour. Technol., 100 (2009) 4127–4132.
[33] P.R. Silva, H.A. Ponte, M.J.J.S. Ponte, N.M.S. Kaminari, Development of a new electrochemical methodology at carbon steel/Na_2S system for corrosion monitoring in oil refineries, J. Appl. Electrochem., 41 (2011) 317–320.
[34] I. Jacukowicz-Sobala, Ł.J. Wilk, K. Drabent, E. Kociołek-Balawejder, Synthesis and characterization of hybrid materials containing iron oxide for removal of sulfides from water, J. Colloid Interface Sci., 460 (2015) 154–163.
[35] I.B. Hariz, L. Monser, Sulfide removal from petroleum refinery wastewater by adsorption on chemically modified activated carbon, Int. Water Technol. J., 4 (2014) 264–267.
[36] S. Agarwal, H. Sadegh, M. Monajjemi, A.S. Hamdy, G.A.M. Ali, A.O.H. Memar, R. Shahryari-Ghoshekandi, I. Tyagi, V.K. Gupta, Efficient removal of toxic bromothymol blue and methylene blue from wastewater by polyvinyl alcohol, J. Mol. Liq., 218 (2016) 191–197.
[37] O.A. Habeeb, K. Ramesh, G.A.M. Ali, R.M. Yunus, Experimental design technique on removal of hydrogen sulfide using CaO-eggshells dispersed onto palm kernel shell activated carbon: experiment, optimization, equilibrium and kinetic studies, J. Wuhan Univ. Technol. Mater. Sci. Ed., 32 (2017) 305–320.
[38] S.J. Allen, G. Mckay, J.F. Porter, Adsorption isotherm models for basic dye adsorption by peat in single and binary component systems, J. Colloid Interface Sci., 280 (2004) 322–333.
[39] G. Limousin, J.-P. Gaudet, L. Charlet, S. Szenknect, V. Barthes, M. Krimissa, Sorption isotherms: a review on physical bases, modeling and measurement, Appl. Geochem., 22 (2007) 249–275.
[40] H.H. Abdel Ghafar, G.A.M. Ali, O.A. Fouad, S.A. Makhlouf, Enhancement of adsorption efficiency of methylene blue on Co_3O_4/SiO_2 nanocomposite, Desal. Water Treat., 53 (2015) 2980–2989.
[41] O.S. Bello, I.A. Adeogun, J.C. Ajaelu, E.O. Fehintola, Adsorption of methylene blue onto activated carbon derived from periwinkle shells: kinetics and equilibrium studies, Chem. Ecol., 24 (2008) 285–295.
[42] V.K. Gupta, S. Agarwal, H. Sadegh, G.A.M. Ali, A.K. Bharti, A.S. Hamdy, Facile route synthesis of novel graphene oxide-β-cyclodextrin nanocomposite and its application as adsorbent for removal of toxic bisphenol A from the aqueous phase, J. Mol. Liq., 237 (2017) 466–472.
[43] F. Haghseresht, G.Q. Lu, Adsorption characteristics of phenolic compounds onto coal-reject-derived adsorbents, Energy Fuels, 12 (1998) 1100–1107.
[44] K.Y. Foo, B.H. Hameed, Insights into the modeling of adsorption isotherm systems, Chem. Eng. J., 156 (2010) 2–10.
[45] M. Hosseini, S.F.L. Mertens, M. Ghorbani, M.R. Arshadi, Asymmetrical Schiff bases as inhibitors of mild steel corrosion in sulphuric acid media, Mater. Chem. Phys., 78 (2003) 800–808.
[46] T.A.S. Elnsar, M.H. Soliman, M.A.-E.-A.A. Ayash, Modified hydroxyapatite adsorbent for removal of iron dissolved in water wells in Sohag, Egypt, Chem. Adv. Mater., 2 (2017) 1–13.
[47] A. Günay, E. Arslankaya, I. Tosun, Lead removal from aqueous solution by natural and pretreated clinoptilolite: adsorption equilibrium and kinetics, J. Hazard. Mater., 146 (2007) 362–371.
[48] A. Dada, A. Olalekan, A. Olatunya, O. Dada, Langmuir, Freundlich, Temkin and Dubinin–Radushkevich isotherms studies of equilibrium sorption of Zn^{2+} unto phosphoric acid modified rice husk, J. Appl. Chem., 3 (2012) 38–45.
[49] H. Sadegh, G.A.M. Ali, V.K. Gupta, A.S.H. Makhlouf, R. Shahryari-ghoshekandi, M.N. Nadagouda, M. Sillanpää, E. Megiel, The role of nanomaterials as effective adsorbents and their applications in wastewater treatment, J. Nanostruct. Chem., 7 (2017) 1–14.
[50] Y.-S. Ho, G. McKay, Sorption of dye from aqueous solution by peat, Chem. Eng. J., 70 (1998) 115–124.
[51] H. Cherifi, B. Fatiha, H. Salah, Kinetic studies on the adsorption of methylene blue onto vegetal fiber activated carbons, Appl. Surf. Sci., 282 (2013) 52–59.
[52] D. Das, D.P. Samal, B. Meikap, Preparation of activated carbon from green coconut shell and its characterization, J. Chem. Eng. Process Technol., 2015 (2015).
[53] C. Pongener, D. Kibami, K.S. Rao, R.L. Goswamee, D. Sinha, Synthesis and characterization of activated carbon from the biowaste of the plant *Manihot esculenta*, Chem. Sci. Trans., 4 (2015) 59–68.
[54] A. Kar, S. Kundu, A. Patra, Photocatalytic properties of semiconductor SnO_2/CdS heterostructure nanocrystals, RSC Adv., 2 (2012) 10222–10230.
[55] Y.-W. Lee, J.-W. Park, S.-J. Jun, D.-K. Choi, J.-E. Yie, NOx adsorption–temperature programmed desorption and surface molecular ions distribution by activated carbon with chemical modification, Carbon, 42 (2004) 59–69.
[56] O.A. Fouad, S.A. Makhlouf, G.A.M. Ali, A.Y. El-Sayed, Cobalt/silica nanocomposite via thermal calcination-reduction of gel precursors, Mater. Chem. Phys., 128 (2011) 70–76.
[57] O.A. Fouad, G.A.M. Ali, M.A.I. El-Erian, S.A. Makhlouf, Humidity sensing properties of cobalt oxide/silica nanocomposites prepared via sol-gel and related routes, Nano, 7 (2012) 1250038–1250049.
[58] G.A.M. Ali, O.A. Fouad, S.A. Makhlouf, Structural, optical and electrical properties of sol-gel prepared mesoporous Co_3O_4/SiO_2 nanocomposites, J. Alloys Compd., 579 (2013) 606–611.
[59] K.Y. Foo, B.H. Hameed, Microwave-assisted preparation and adsorption performance of activated carbon from biodiesel industry solid reside: influence of operational parameters, Bioresour. Technol., 103 (2012) 398–404.
[60] M. Florent, R. Wallace, T.J. Bandosz, Removal of hydrogen sulfide at ambient conditions on cadmium/GO-based composite adsorbents, J. Colloid Interface Sci., 448 (2015) 573–581.
[61] X. Xu, X. Cao, L. Zhao, T. Sun, Comparison of sewage sludge- and pig manure-derived biochars for hydrogen sulfide removal, Chemosphere, 111 (2014) 296–303.
[62] M.S. El-Geundi, Homogeneous surface diffusion model for the adsorption of basic dyestuffs onto natural clay in batch adsorbers, Adsorpt. Sci. Technol., 8 (1991) 217–225.
[63] J. Kazmierczak-Razna, B. Gralak-Podemska, P. Nowicki, R. Pietrzak, The use of microwave radiation for obtaining activated carbons from sawdust and their potential application in removal of NO_2 and H_2S, Chem. Eng. J., 269 (2015) 352–358.
[64] S. Asaoka, H. Okamura, R. Morisawa, H. Murakami, K. Fukushi, T. Okajima, M. Katayama, Y. Inada, C. Yogi, T. Ohta, Removal of hydrogen sulfide using carbonated steel slag, Chem. Eng. J., 228 (2013) 843–849.
[65] Y. Xiao, S. Wang, D. Wu, Q. Yuan, Experimental and simulation study of hydrogen sulfide adsorption on impregnated activated carbon under anaerobic conditions, J. Hazard. Mater., 153 (2008) 1193–1200.
[66] R. Wallace, M. Seredych, P. Zhang, T.J. Bandosz, Municipal waste conversion to hydrogen sulfide adsorbents: investigation of the synergistic effects of sewage sludge/fish waste mixture, Chem. Eng. J., 237 (2014) 88–94.
[67] M. Seredych, T.J. Bandosz, Adsorption of hydrogen sulfide on graphite derived materials modified by incorporation of nitrogen, Mater. Chem. Phys., 113 (2009) 946–952.

[68] D. Nguyen-Thanh, T.J. Bandosz, Activated carbons with metal containing bentonite binders as adsorbents of hydrogen sulfide, Carbon, 43 (2005) 359–367.
[69] M. Seredych, C. Portet, Y. Gogotsi, T.J. Bandosz, Nitrogen modified carbide-derived carbons as adsorbents of hydrogen sulfide, J. Colloid Interface Sci., 330 (2009) 60–66.
[70] A. Bagreev, T.J. Bandosz, H_2S adsorption/oxidation on unmodified activated carbons: importance of prehumidification, Carbon, 39 (2001) 2303–2311.
[71] A. Bagreev, J.A. Menendez, I. Dukhno, Y. Tarasenko, T.J. Bandosz, Bituminous coal-based activated carbons modified with nitrogen as adsorbents of hydrogen sulfide, Carbon, 42 (2004) 469–476.
[72] S. Montoya-Suarez, F. Colpas-Castillo, E. Meza-Fuentes, J. Rodríguez-Ruiz, R. Fernandez-Maestre, Activated carbons from waste of oil-palm kernel shells, sawdust and tannery leather scraps and application to chromium (VI), phenol, and methylene blue dye adsorption, Water Sci. Technol., 73 (2016) 21–27.
[73] A. Jumasiah, T.G. Chuah, J. Gimbon, T.S.Y. Choong, I. Azni, Adsorption of basic dye onto palm kernel shell activated carbon: sorption equilibrium and kinetics studies, Desalination, 186 (2005) 57–64.
[74] Y.B. Onundi, A.A. Mamun, M.F.A. Khatib, Y.M. Ahmed, Adsorption of copper, nickel and lead ions from synthetic semiconductor industrial wastewater by palm shell activated carbon, Int. J. Environ. Sci. Technol., 7 (2010) 751–758.